Emergence of Hexagonally Close-Packed Spheres in Linear Block Copolymer Melts

Cheng Zhang,^{†,F,I} Daniel L. Vigil,[†] Dan Sun,[†] Morgan W. Bates,[†] Tessa Loman,[†] Elizabeth A. Murphy,[†] Stephanie M. Barbon,[†] Jung-Ah Song,[†] Beihang Yu,[§] Glenn H. Fredrickson,^{†,‡,§} Andrew K. Whittaker,*,^{F,I} Craig J. Hawker,*,^{†,‡,%} and Christopher M. Bates*,^{‡,†,§,%}

†Materials Research Laboratory, ‡Materials Department, and §Department of Chemical Engineering, %Department of Chemistry & Biochemistry, University of California, Santa Barbara, California 93106, United States ^IAustralian Institute for Bioengineering and Nanotechnology, ^IARC Centre of Excellence in Convergent Bio-Nano Science and Technology, University of Queensland, Brisbane, Queensland 4072, Australia

ABSTRACT

The hexagonally close-packed (HCP) sphere phase is predicted to be stable across a narrow region of linear block copolymer phase space, but the small free energy difference separating it from face-centered cubic spheres usually results in phase coexistence. Here, we report the discovery of pure HCP spheres in linear block copolymer melts with A = poly(2,2,2-trifluoroethyl)acrylate) ("F") and B = poly(2-dodecyl acrylate) ("2D") or poly(4-dodecyl acrylate) ("4D"). In 4DF diblocks and F4DF triblocks, the HCP phase emerges across a substantial range of A-block volume fractions (circa $f_A = 0.25-0.30$), and in F4DF it forms reversibly when subjected to various processing conditions which suggests an equilibrium state. The timescale associated with forming pure HCP upon quenching from a disordered liquid is intermediate to the ordering kinetics of the Frank-Kasper σ and A15 phases. However, unlike σ and A15, HCP nucleates directly from a supercooled liquid or soft solid without proceeding through an intermediate quasicrystal. Selfconsistent field theory calculations indicate the stability of HCP is intimately tied to small amounts of molar mass dispersity (*D*); for example, an HCP-forming F4DF sample with $f_A = 0.27$ has an experimentally measured D = 1.04. These insights challenge the conventional wisdom that pure HCP is difficult to access in linear block copolymer melts without the use of blending or other complex processing techniques.

FOR TABLE OF CONTENTS USE ONLY

INTRODUCTION

The optimal packing of solids into periodic and aperiodic structures has fascinated mathematicians for centuries with implications across nearly all fields of science, from chemistry to physics. Perhaps the simplest example relates to the conjecture offered by Kepler in 1611, which states the densest packing of equal-volume hard spheres is approximately 74.05% in 3 dimensions corresponding to layers with *p6mm* plane-group symmetry that stack in a face-centered-cubic ("FCC": ABCABC...) or hexagonally-close-packed ("HCP": ABAB...) sequence. Remarkably, despite contributions from Carl Gauss and inclusion in Hilbert's famous *Twenty-Three Unsolved Problems in Mathematics* (1900), the Kepler conjecture took nearly 400 years to prove, a feat finally achieved by Thomas Hales in 1998. The importance of this packing problem is by no means insignificant—many materials governed by seemingly distinct physical interactions tend to favor the formation of FCC and HCP densely packed solids, from marbles in a jar to the atomic crystal structure of elements and alloys.^{1,2}

A marked difference arises when the spheres have a soft shell with configurational entropy. In such cases, body-centered cubic (BCC) symmetry (space group $Im\bar{3}m$) often emerges instead of FCC ($Fm\bar{3}m$) or HCP ($P6_3/mmc$) as exemplified by a host of soft materials, including polymer-functionalized nanoparticles³ and lyotropic liquid crystals.⁴ This trend is particularly evident in the phase behavior of block copolymers, which has attracted significant attention over the past ~50 years due to a convergence of enabling synthetic methods and theoretical advances.⁵ The conventional melt phase behavior of block copolymers—parametrized by the volumetric degree of polymerization (N), Flory–Huggins interaction parameter (χ), and block volume fractions (f_A , f_B , ...)—is dominated by four morphologies: BCC spheres, hexagonally-packed cylinders (HEX), the double gyroid network, and lamellae.^{5,6} (Recent experiments have also

identified two equilibrium Frank–Kasper phases, σ^7 and A15,⁸ at elevated values of conformational asymmetry, $\varepsilon > 1$.) Close-packed sphere (CPS) phases (HCP and FCC) are predicted by self-consistent field theory (SCFT) to be stable in several variations of branched block copolymer melts, including (BAB)_n stars,⁹ AB_n miktoarms,^{10,11} and ABA_T¹² or (B_T)AB(A_T) tethered copolymers,¹³ but they are almost entirely absent from monodisperse linear block copolymer phase diagrams¹⁴ because of "packing frustration."^{15,16} This concept is based on the energetic dichotomy of (1) minimizing A–B interfacial area and (2) maintaining uniform chain stretching. In the case of particle phases, the former favors spherical interfaces, while the latter is optimized when the A–B interface deforms to match the shape of its local Wigner–Seitz cell. These two extremes are clearly at odds and the BCC phase ends up being lower in free energy than HCP and FCC since it has a more spherical Wigner–Seitz cell—a truncated octahedron.¹⁷

Although the BCC phase dominates sphere-forming regions of linear block copolymer phase diagrams, CPS phases *are* predicted to occur in a small area bordering the disordered state at extreme compositions (f_A or $f_B \ll 0.5$). In pioneering work, Huang and coworkers provide a sense of how limiting these constraints are: a single poly(ethylene oxide)-b-poly(1,4-butadiene) (PEO-b-PBD) diblock copolymer ($M_n = 14.7$ kDa, D = 1.05, $f_{PEO} = 0.18$) self-assembled into coexisting CPS and disordered micelles over a temperature range of about 4 °C. ¹⁸ (We note that the original publication identified this CPS phase as FCC, the purity of which was later called into question. ^{19,20}) Hsu recently reexamined the phase behavior of PEO-b-PBD with a significantly lower molecular weight ($M_n = 3$ kDa, D = 1.04, $f_{PEO} = 0.167$) and identified a slow transformation from BCC to HCP spheres over the course of 120 h at 27 °C, which persisted across a slightly larger temperature range to ~40 °C. ²⁰ This result is rather surprising; even though SCFT calculations indicate the HCP is globally stable, conventional wisdom suggests experimentalists

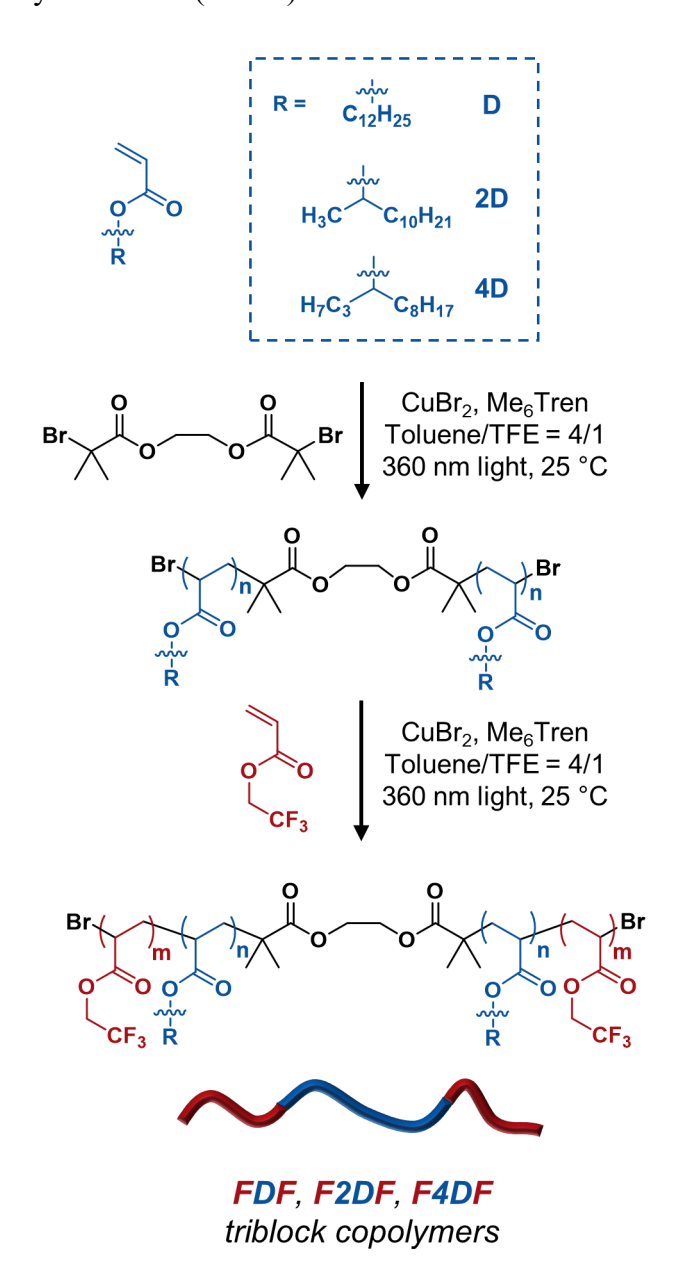
are unlikely to find pure FCC or HCP because the free energy difference separating them is vanishingly small.¹⁹

The formation of close-packed spheres at extreme compositions near the order–disorder transition is related to chain pullout, which relieves packing frustration by filling the far reaches of Wigner–Seitz cells with compositionally asymmetric chains that approximate homopolymer. This effect can be amplified to further stabilize CPS phases by adding solvent²¹⁻²⁴ or homopolymer chains,²⁵⁻²⁷ increasing the molar mass dispersity of a block copolymer,^{15,28} or applying external fields (e.g., shear or flow).^{29,30} Experimentally, these techniques often sacrifice long-range order or involve complex processing that results in the transient formation of coexisting FCC and HCP. To the best of our knowledge, there are no efficient ways of stabilizing a pure HCP phase in quiescent block copolymer melts across substantial portions of χN – f_A space.

Here, we demonstrate through a combination of synthesis, characterization, and theory, that linear block copolymers can form pure HCP sphere phases over a wide range of compositions $(f_A \approx 0.25\text{--}0.30)$ and temperatures $(T \approx 25\text{--}180 \,^{\circ}\text{C})$ with the appropriate choice of A- and B-block chemistry. Our primary analysis focuses on a series of symmetric ABA triblocks with A = poly(2,2,2-trifluoroethyl acrylate) ("F") and three different midblocks: B = poly(dodecyl acrylate) ("D"), poly(2-dodecyl acrylate) ("2D"), or poly(4-dodecyl acrylate) ("4D"). These materials show surprisingly different self-assembly; while FDF forms a mixture of FCC and BCC across a limited range of compositions at $f_F \ll 0.5$, switching the B block to F2DF or especially F4DF results in large regions of pure HCP. Similar results are observed with an analogous poly(4-dodecyl acrylate)–block—poly(2,2,2-trifluoroethyl acrylate) diblock ("4DF"), suggesting the choice of monomers is crucial for stabilizing a pure HCP phase. This effect cannot be captured by SCFT, but mean-field calculations do hint at important mechanisms that stabilize HCP. Critically,

properly accounting for very small amounts of dispersity leads to good agreement between theory and experiments. These studies reveal surprising new insights into the formation of a pure and readily accessible hexagonally close-packed sphere phase in linear block copolymer melts.

Scheme 1. Synthesis of FDF, F2DF, and F4DF triblock copolymers via sequential photo-mediated atom transfer radical polymerization (ATRP).



RESULTS AND DISCUSSION

Synthesis

Before discussing the serendipitous discovery of a stable and pure HCP phase in linear copolymer melts, we briefly describe the synthesis of various ABA triblock and AB diblock copolymers. Three types of symmetric ABA triblock copolymers were synthesized via sequential photo-mediated atom-transfer radical polymerization (ATRP) starting from the bifunctional initiator 1,2-bis(bromoisobutyryloxy)ethane (BBiBE, Scheme 1, Figure S1): poly(2,2,2trifluoroethyl acrylate)-block-poly(dodecyl acrylate)-block-poly(2,2,2-trifluoroethyl acrylate) ("FDF"), poly(2,2,2-trifluoroethyl acrylate)—block—poly(2-dodecyl acrylate)—block—poly(2,2,2trifluoroethyl acrylate) ("F2DF"), and poly(2,2,2-trifluoroethyl acrylate)-block-poly(4-dodecyl acrylate)—block—poly(2,2,2-trifluoroethyl acrylate) ("F4DF"). This is a convenient synthetic platform with the same reaction conditions being used for each A/B monomer pair, yielding materials with low molar mass dispersities and high chain-end fidelity. See the Supporting Information for details regarding the synthesis of 2-dodecyl acrylate and 4-dodecyl acrylate monomers by esterification of commercially available alcohols with acryloyl chloride (Figures S2 and S3). 31,32 Libraries of FDF, F2DF, and F4DF triblock copolymers, as well as analogous 4DF diblock copolymers, were synthesized across a range of F volume fractions ($f_F \approx 0.15-0.55$). Figure 1 shows representative size-exclusion chromatograms (SECs) of three triblock copolymers—FDF-28, F2DF-27, F4DF-27—which will be the focus of our analysis below. Note that our sample nomenclature FXF-YY defines X as the type of B block (D, 2D, or 4D) and YY as the F-block volume percent (i.e., $f_F \times 100$). See the Supporting Information for complete characterization data of the entire sample library (Figures S4–S7 and Tables S1–S4). In summary,

the SEC traces of all block copolymers and their macromonomer precursors were monomodal and reasonably symmetric with low molar-mass dispersities ($D \le 1.15$).

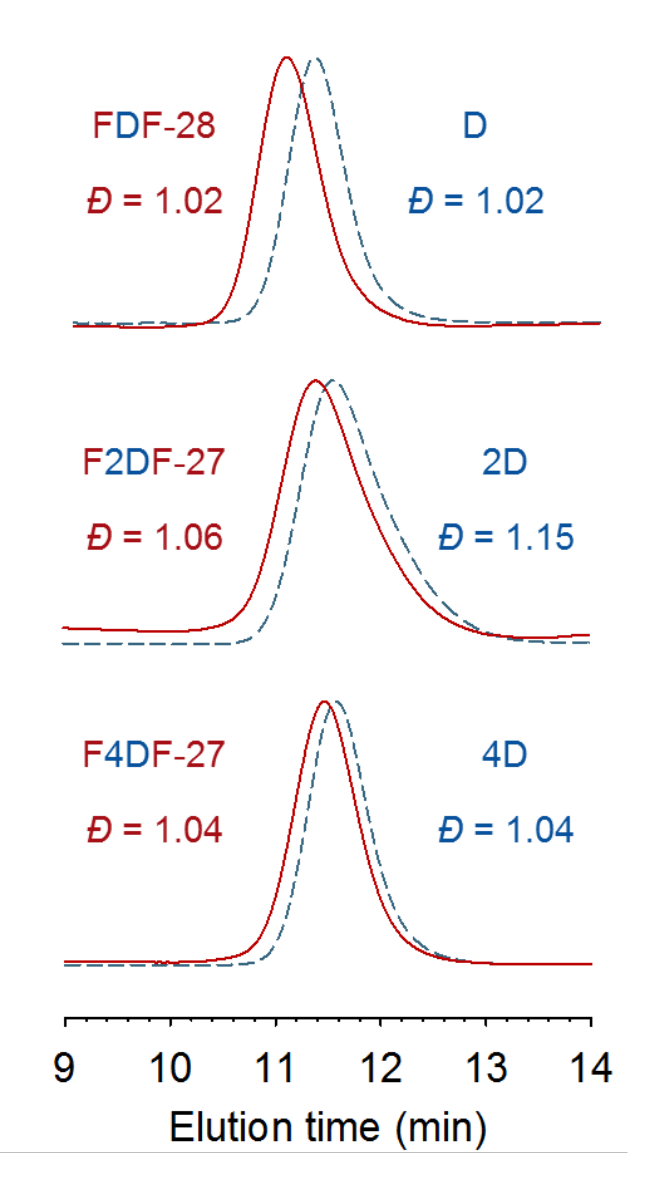


Figure 1. SECs (normalized differential refractive index signal) of representative triblock copolymers FDF-28, F2DF-27, and F4DF-27 prepared by sequential photo-mediated ATRP from a bifunctional initiator. D, 2D and 4D were polymerized first (dashed blue lines) followed by growth of the outer poly(trifluoroethyl acrylate) F blocks (solid red lines). See **Table 1** and the Supporting Information (Tables S1–S3) for a comprehensive tabulation of characterization data.

Table 1. Molecular characterization of representative FXF (X = D, 2D, 4D) triblock copolymers.

Entry	DP_X^a	$DP_{\mathrm{F}}{}^{\mathrm{b}}$	$M_{\rm n,BP}^{\rm c}$ (g/mol)	$ ot\! D^{\mathrm{d}}$	$f_{\rm F}^{\rm e}$	N^{f}	$T_{\mathrm{ODT}^{\mathrm{g}}}(^{\circ}\mathrm{C})$
FDF-28	43	38	16,500	1.02	0.28	213	110
F2DF-27	44	39	16,900	1.06	0.27	219	108
F4DF-27	42	33	15,400	1.04	0.27	183	132

^aNumber-average degree of polymerization of the *X* precursor (D, 2D, or 4D) from multi-angle laser light scattering size-exclusion chromatography (MALLS-SEC) analysis in THF. ^bF-block number-average degree of polymerization calculated by ¹H NMR analysis of the triblock copolymer. ^cTotal molar mass of the block copolymer. ^dMolar mass dispersity determined using MALLS-SEC. ^eVolume fraction of F based on measured homopolymer densities (see Table S5) and ¹H NMR. ^fTotal volumetric degree of polymerization based on homopolymer densities and a reference volume of 118 Å³. ^gOrder–disorder transition temperature determined from DMTA performed on heating at a rate of 2 °C/min.

Phase Behavior

Phase diagrams were constructed for FDF, F2DF, and F4DF using a combination of small-angle X-ray scattering (SAXS) to interrogate self-assembly (Figures S8–S14) and dynamic mechanical thermal analysis (DMTA, Figure S15) to measure order–disorder transition temperatures ($T_{\rm ODT}$) by monitoring changes in G' on slow heating (2 °C/min) at a fixed low frequency ($\omega = 1$ rad/s). To map volumetric degree of polymerizations (N) onto segregation strength (χN), the Flory–Huggins interaction parameter $\chi = \alpha/T + \beta$ of each monomer pair was determined from experimentally measured $T_{\rm ODT}$ values for a series of compositionally symmetric samples ($f_{\rm F} \approx 0.5$) using the mean-field result for symmetric triblock copolymers: (χN)_{ODT} = 18.996.^{33,34} See the Supporting Information (Figure S16) for details of our analysis by linear regression, which yielded the following expressions: $\chi_{\rm FDF} = (84 \pm 1)/T - (0.101 \pm 0.003)$, $^{35}_{\chi \rm F2DF} = (77 \pm 7)/T - (0.06 \pm 0.03)$, and $\chi_{\rm F4DF} = (59 \pm 5)/T + (0.02 \pm 0.01)$. Note that the FDF expression was previously reported and is reproduced here for comparison. 35

Figure 2 summarizes the phase behavior of FDF, F2DF, and F4DF at minority F-block volume fractions ($f_F < 0.5$). A number of unique features are apparent, most notably regions of pure HCP found with F2DF and F4DF triblocks, which is also observed in 4DF diblocks (Figure S11). Figure 3a shows a synchrotron SAXS pattern of F4DF-27 obtained after thermal annealing at 120 °C for 14 h. This phase is pure as evidenced by the close agreement between the Bragg peaks present and those expected for space group $P6_3/mmc$ (#194) with Wyckoff position 2coccupied. Although HCP and FCC share many Bragg reflections that occur at identical magnitudes of the scattering wave vector (q) when the interlayer spacing is matched ($d_{(002),HCP} = d_{(111),FCC}$), unique reflections that would be expected for space group $Fm\bar{3}m$ (#225) with Wyckoff position 4a occupied are absent. For example, if FCC were in coexistence with HCP, its {200} family of reflections would appear as a shoulder to the right of the predominant HCP triplet, which is not observed (Figure S17). The high purity of this HCP phase allowed us to reconstruct the real-space electron-density distribution from the one-dimensional SAXS data using an established procedure: the magnitude of each reciprocal lattice vector was fit with Le Bail refinement (Figure S18) followed by charge flipping to circumvent the crystallographic phase problem.^{8,36} Hexagonal symmetry is apparent when projected down the c axis (Figure 3b), as is the AB layer stacking when viewed along (100] (Figure 3c). Note that these two depictions of the unit cell are false colored to emphasize the alternating layer stacking; each micelle is necessarily identical and related by symmetry operations. Notable distortion of the micelles is also evident, for example, along (120].

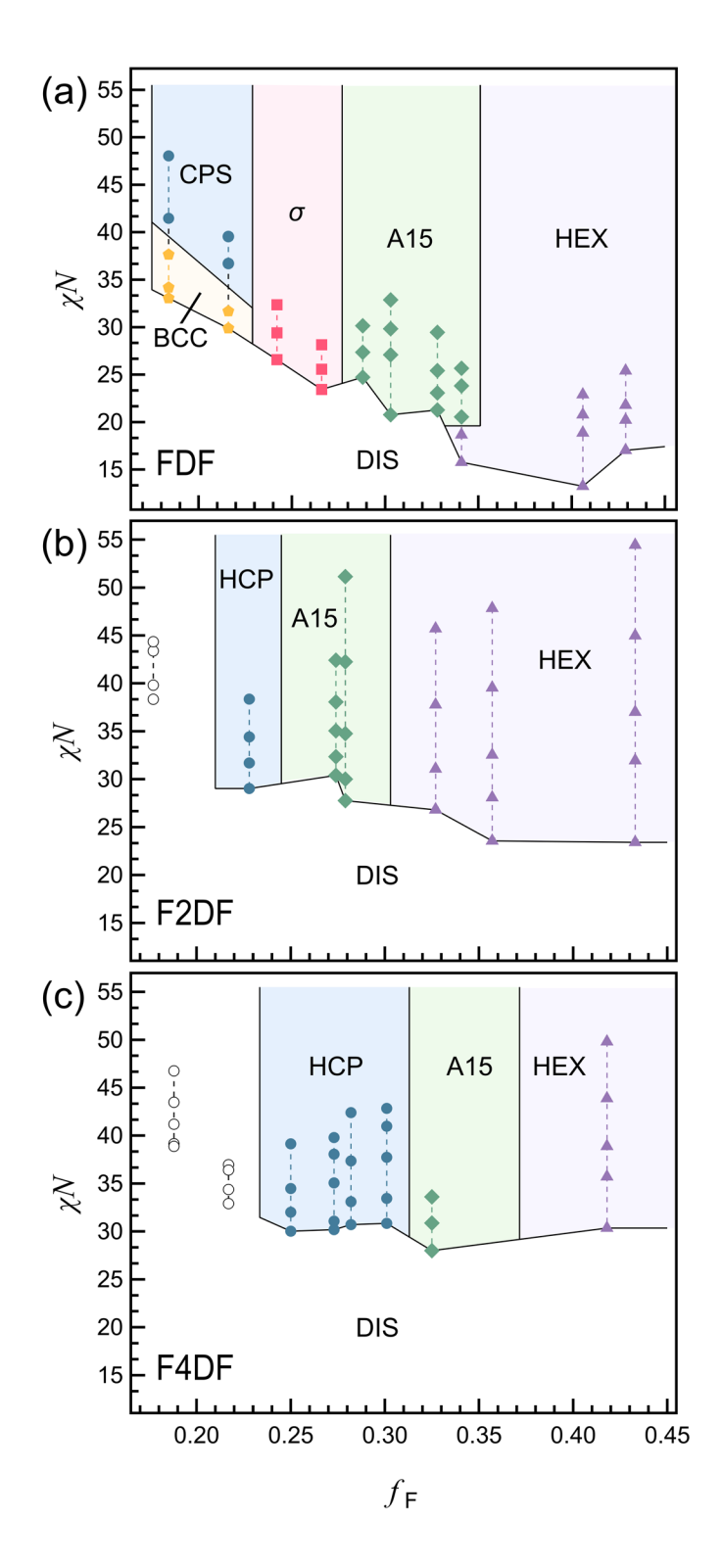


Figure 2. Phase diagrams for FDF, F2DF and F4DF triblock copolymers. Note that we previously reported the FDF phase diagram,³⁵ which is reproduced here for comparison. See the Supporting Information for SAXS patterns, an estimation of χ parameters, and the measurement of $T_{\rm ODT}$ values.

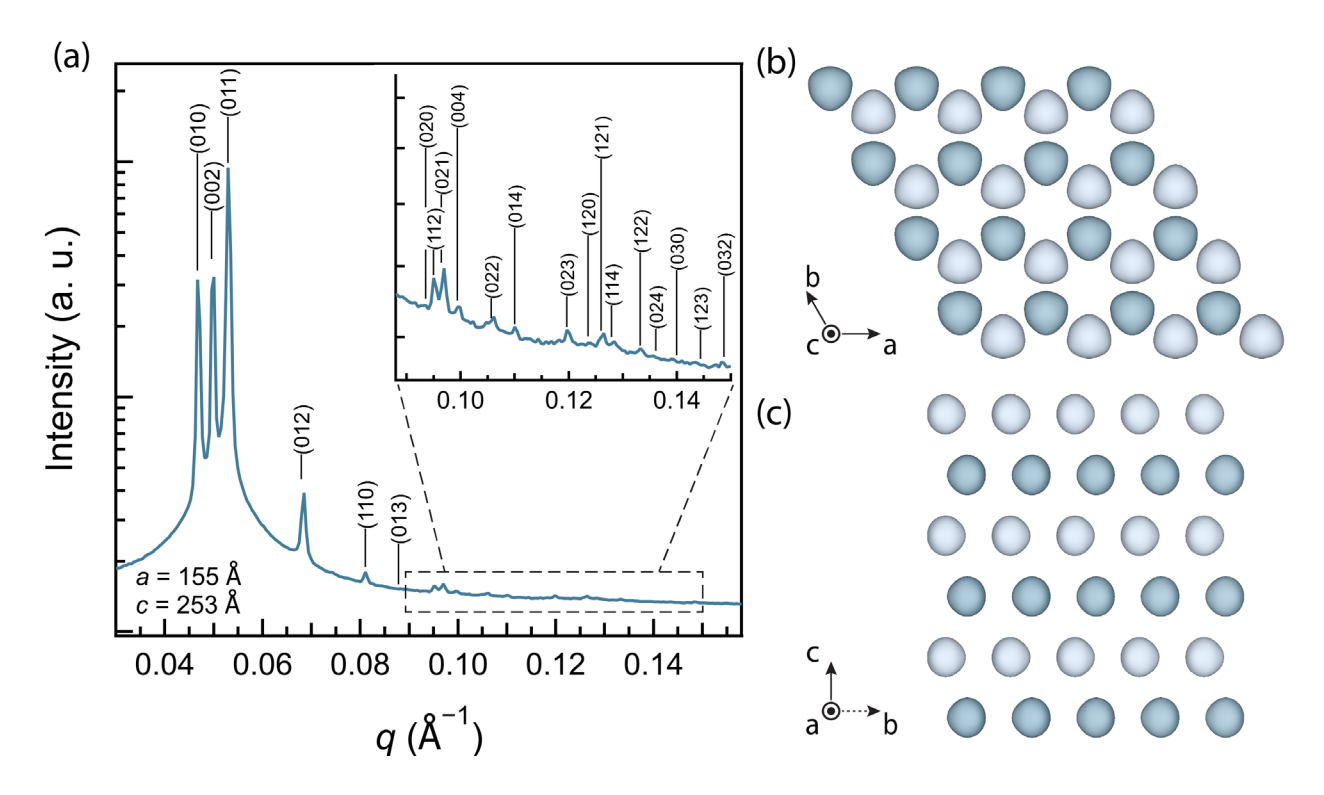


Figure 3. (a) F4DF-27 forms a pure HCP sphere phase as evidenced by SAXS obtained after thermal annealing at 120 °C for 14 h. **(b,c)** Unit cell electron density reconstruction from the one-dimensional SAXS data shown in (a); (b) and (c) are unit cell projections of the electron density map along the c and a axis, respectively. False coloring highlights alternating layers of aggregated F blocks ($f_F = 0.27$) which are actually symmetry-equivalent, occupying Wyckoff position 2c. 4D blocks fill the remaining space between micelles.

The phase diagrams in **Figure 2** also reveal channels of stability for two complex spherical packings— σ and A15—that are members of the infinite family of Frank–Kasper phases. σ and A15 have recently been established as equilibrium phases in AB-type block copolymer melts, including AB diblocks,^{7,8,37} ABA triblocks,³⁵ (AB)_n radial stars,^{9,35} and AB_n miktoarm stars.^{10,11,38,39} These structures emerge when copolymers have non-negligible conformational asymmetry (ε), a parameter that captures the tendency of each block to fill space unequally on either side of the A–B interface. We have previously estimated the conformational asymmetry of

FDF as $\varepsilon_{\text{FD}} = b_{\text{F}}/b_{\text{D}} = 1.43$, where b_i is the statistical segment length of block i as calculated from the entanglement plateau measured by rheology.³⁵ Here, we attempted to perform a similar analysis to estimate ε_{F2D} and ε_{F4D} but encountered difficulties synthesizing the homopolymers of 2-dodecyl acrylate and 4-dodecyl acrylate with sufficiently high molecular weight (> 100 kDa) to show a prominent entanglement plateau. Nevertheless, the fact that A15 appears in the F2DF and F4DF phase diagrams strongly suggests ε_{F2D} and ε_{F4D} are comparable to ε_{FD} , as the stabilization of the A15 phase requires even higher values of ε than the σ phase.

Another striking feature of the FDF, F2DF, and F4DF phase diagrams in **Figure 2** is their markedly different phase portraits. As we previously reported, the phase diagram of FDF roughly follows expectations;³⁵ sphere phases traverse the sequence BCC $-\sigma$ -A15 as f_F increases. (We note in passing that samples at low f_F show a reversible, temperature-dependent CPS-BCC order-order transition that is counter to theoretical predictions.³⁵) In contrast, F2DF and F4DF both form pure HCP but with different windows of stability. F2DF self-assembles into pure HCP at a single composition ($f_F = 0.23$, Figure S9) and four different F4DF samples did so spanning at least 5 volume percent ($f_F = 0.25$ -0.30, Figure S10). While the precise location of order-order phase boundaries is not currently known, it is clear that the HCP window in F4DF significantly intrudes on the σ phase. Similarly, the formation of pure HCP was also observed in three different 4DF diblock samples ($f_F = 0.23$ -0.29, Figure S11).

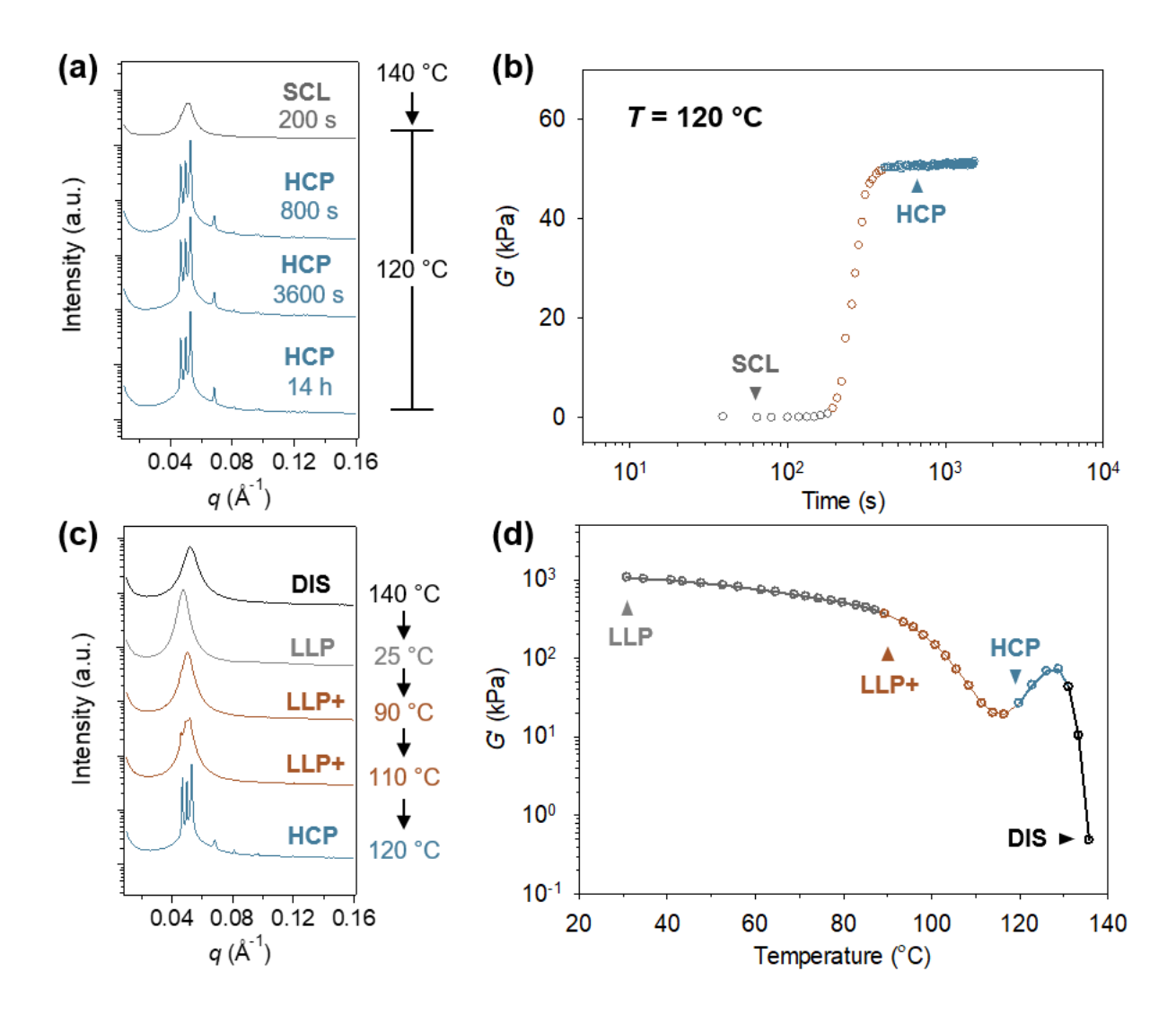


Figure 4. The pure HCP phase found in F4DF-27 ($T_{ODT} = 132 \,^{\circ}$ C) forms irrespective of processing conditions, suggesting an equilibrium state. (**a,b**) Time-dependent (**a**) synchrotron SAXS and (**b**) DMTA measurements after rapid quenching from the disordered state ($T > T_{ODT}$) to 120 °C. (**c,d**) Temperature-dependent (**c**) synchrotron SAXS and (**d**) DMTA ($\gamma = 1\%$ and $\omega = 1 \, \text{rad/s}$) measured upon heating from 25 °C to T_{ODT} at 15 °C/min. Prior to the measurements in (**c**) and (**d**), samples were rapidly quenched from the disordered state to 25 °C at 15 °C/min. SAXS patterns were collected sequentially from top to bottom at each temperature as indicated and have been shifted vertically for clarity. Legend: DIS = disordered, SCL = supercooled liquid, LLP = liquid-like packing, LLP+ = liquid-like packing coexisting with an ordered morphology, HCP = pure hexagonally close-packed spheres.

Time- and temperature-dependent experiments indicate the pure HCP phase found in F4DF-27 forms irrespective of processing conditions. Figure 4a,b shows SAXS and DMTA experiments that follow the ordering kinetics of F4DF-27 after directly quenching from $T > T_{ODT}$ to T = 120 °C ($T_{\text{ODT}} - T \approx 10$ °C) at a rate of approximately 100 °C/min. As evidenced by SAXS (Figure 4a), a clean HCP phase quickly nucleates and grows within 800 s from the disordered, supercooled liquid (SCL) state. This scattering pattern remains unchanged over 14 h. Analogous processing was performed by DMTA (Figure 4b), which indicates a gradual increase in the storage modulus G' as a function of time. We interpret this stiffening as representing the transformation from a supercooled liquid with $G' \sim 0$ to an ordered, soft-solid (HCP). G' plateaus on a timescale that is consistent with the SAXS measurements, and the fact that it stops changing further supports the inference that the resulting HCP phase is stable. A complementary set of temperaturedependent experiments was also performed to probe the formation of HCP on heating. F4DF-27 was first cooled from the disordered state ($T > T_{\rm ODT}$) to 25 °C at 15 °C/min, followed by monitoring the morphology (Figure 4c) and dynamic response (Figure 4d) on heating at 15 °C/min with SAXS and DMTA, respectively. At 25 °C, F4DF-27 exhibits liquid-like packing (LLP), which we note is characteristic of a disordered solid ($G' \gg 0$) rather than a disordered liquid (SCL, $G' \sim 0$).¹⁷ Upon heating, the LLP state directly transforms into HCP at $T \sim 120$ °C as demonstrated by the formation of sharp Bragg reflections in the SAXS pattern and additional stiffening measured by DMTA. Further heating the sample leads to disordering at approximately $T_{\rm ODT} = 132$ °C. In summary, with F4DF-27, different processing pathways all yield HCP spheres, suggesting it is indeed an equilibrium morphology.

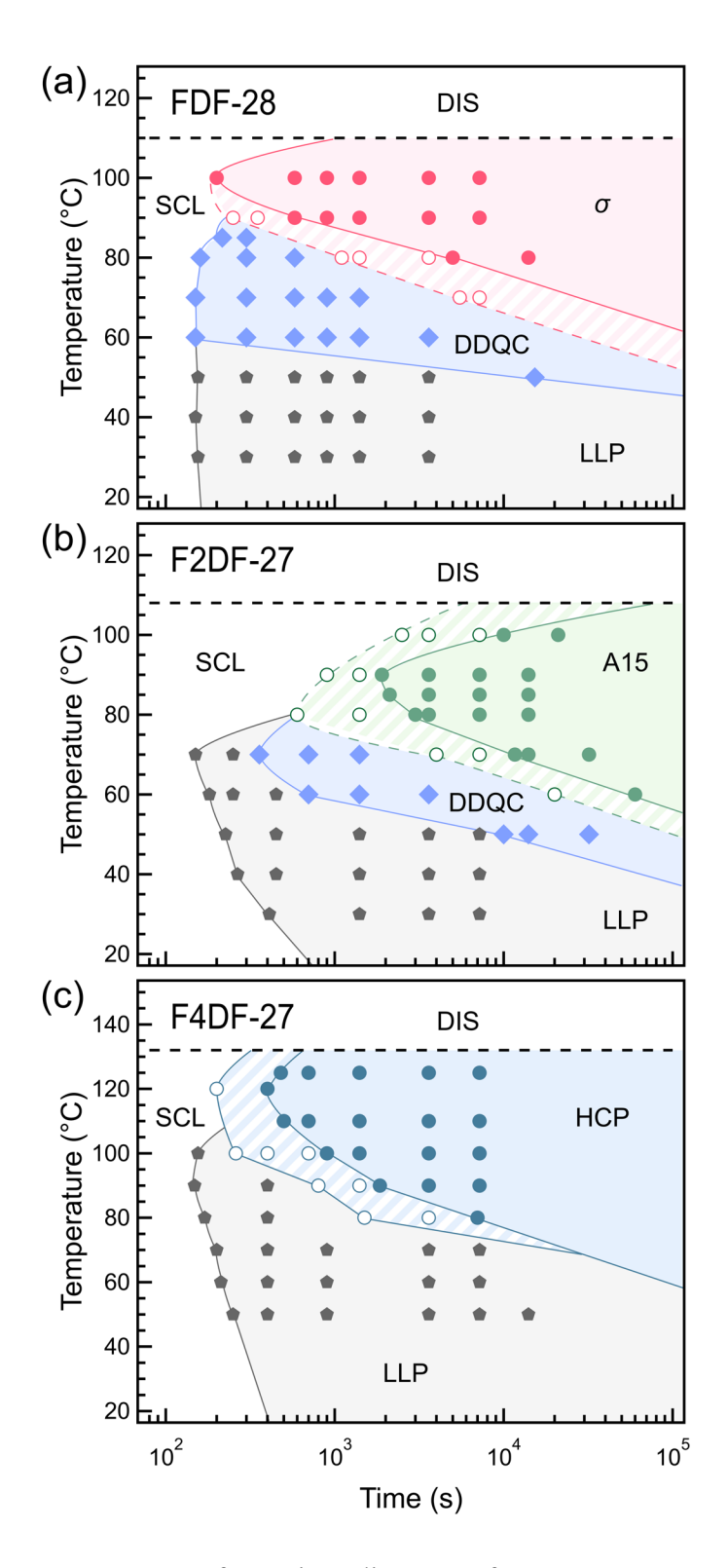


Figure 5. Time–temperature–transformation diagrams for FDF-28, F2DF-27, and F4DF-27 indicate the HCP phase nucleates directly from a supercooled liquid, unlike σ and A15 that proceed through an intermediate dodecagonal quasicrystal (DDQC). The kinetics of ordering were

determined by time-dependent SAXS and DMTA after rapidly cooling from $T > T_{\text{ODT}}$ at a rate of approximately 100 °C/min. Filled circles represent σ (red circle), A15 (green circle), HCP (navy blue circle), DDQC (light blue square), and LLP (grey pentagon). Empty circles signify phase coexistence that occurs during gradual nucleation and growth. Solid and dashed lines are guides to the eye. Order–disorder transition temperatures are indicated by horizontal dashed lines.

Our ability to controllably and reversibly form HCP allows the ordering kinetics of this close-packed sphere phase to be compared with more complex Frank-Kasper analogues. Figure 5 shows time-temperature-transformation (TTT) diagrams for FDF-28, F2DF-27, and F4DF-27, which were constructed using a combination of SAXS and DMTA as outlined above (see also Figures S19–S23). These samples have nearly identical volume fractions and molecular weights (**Table 1**) but very different phase behavior (**Figure 2**); at long times, FDF-28 (σ) and F2DF-27 (A15) self-assemble into Frank-Kasper phases, while F4DF-27 forms HCP. The most salient feature of Figure 5 is the dodecagonal quasicrystal (Figures S24–S25) that transiently forms in FDF-28 and F2DF-27 at deep quench depths between SCL (or LLP at lower temperatures) and the equilibrium Frank-Kasper phase (σ or A15). In contrast, there is no evidence of quasicrystal formation in F4DF-27, which proceeds directly from SCL or LLP to HCP. These results are consistent with Frank-Kasper phases being closely related to two-dimensional quasicrystals, while HCP is not. Figure 5 also contains interesting implications about the relative ordering kinetics of various sphere phases in samples with nearly identical molecular weights and compositions (Table 1). Comparing the fastest ordering time or "nose" of each TTT diagram (i.e., $T \approx 100$ °C and $t \approx$ 200 s for FDF-28; $T \approx 90$ °C and $t \approx 2000$ s for F2DF-27; $T \approx 120$ °C and $t \approx 400$ s for F4DF-27), which represents the optimal combination of nucleation and growth, ^{17,40} the A15 phase (Figure **5b**, F2DF-27) forms about one order of magnitude slower than σ , with HCP intermediate between

the two. The origin of these rate differences may be related to intrinsic characteristics of each phase. A15, σ , and HCP have variable numbers of symmetry-distinct micelles per unit cell (2, 5, and 1, respectively), which adjust shape and volume while approaching equilibrium. However, the samples in **Figure 5** also have different segregation strengths at their respective noses: $(\chi N)_{100^{\circ}\text{C}} = 26 \text{ (FDF-}28, \sigma) < (\chi N)_{120^{\circ}\text{C}} = 31 \text{ (F4DF-}27, HCP) < (\chi N)_{90^{\circ}\text{C}} = 33 \text{ (F2DF-}27, A15)}$. This relative ordering suggests diffusion effects are at least partly responsible for the range of observed ordering times since the diffusion constant scales as $D \sim \exp(-\chi N)$. The different bulkiness of each midblock (D, 2D, and 4D) may also impact the relative ordering time of each phase by changing the monomer friction coefficient. Nevertheless, the kinetic data in **Figure 5** offer a glimpse at the relevant timescales associated with forming various spherical phases in similar block copolymer melts.

Origins of HCP Stability

The appearance of pure HCP in **Figures 2–5** is surprising from two standpoints. First, the HCP and FCC phases are theoretically separated by such a small difference in free energy per chain ($\sim 10^{-4}kT$) that one would intuitively expect phase coexistence.¹⁹ This order of magnitude is even smaller than the difference between various Frank–Kasper phases ($\sim 10^{-3}kT$), which are susceptible to kinetic trapping during processing.⁴² Yet we find no hints that processing influences the formation or long-term stability of a pure HCP phase (**Figure 4**). Second, from a chemistry perspective, the phase diagrams of FDF, F2DF, and F4DF are strikingly different (**Figure 2**) despite their remarkably similar chemical structures; the pendant groups of each mid-block (D, 2D, and 4D) are simple constitutional isomers of $C_{12}H_{25}$ (**Scheme 1**).

To better understand the origins of HCP stability, we constructed an SCFT model meant to mimic FDF, F2DF, and F4DF triblocks. We initially suspected that conformational asymmetry

might account for the differences in phase behavior. Consequently, F end blocks were modeled as linear freely jointed chains while the central block was modeled as a freely jointed chain with one or two pendant groups on each backbone bead. See the Supporting Information for more details. As shown in **Figure 6**, SCFT calculations on monodisperse melts (D = 1.00) predict very similar order–order phase boundaries across the series of triblocks. Moreover, there is strong disagreement between the monodisperse calculations and the experimental F4DF phase diagram: SCFT predicts narrow regions of HCP and BCC, a large σ window, and no A15. (We note that the A15 discrepancy is likely related to SCFT overestimating the amount of conformational asymmetry necessary to stabilize Frank–Kasper phases.⁸) As a result, conformational asymmetry is clearly not responsible for the phase behavior observed experimentally.

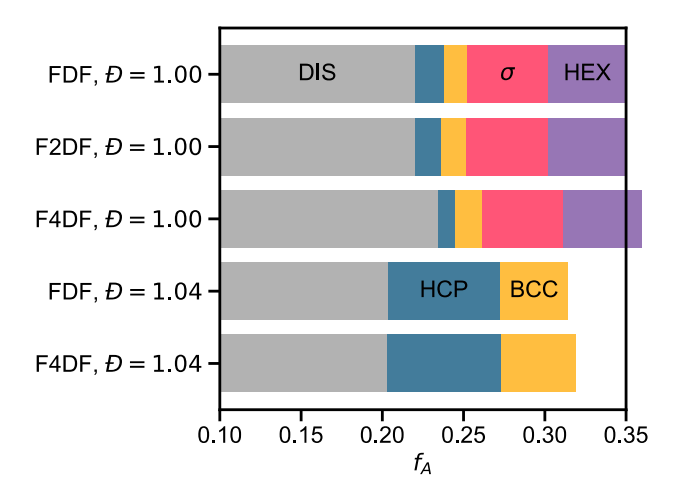


Figure 6. SCFT phase diagram at $\chi N = 40$ for monodisperse (D = 1.00) and slightly disperse (D = 1.04) triblock copolymer melts.

Previous calculations by Matsen have indicated appreciable molar mass dispersity (D > 1.2) in the A block of AB diblock¹⁵ or BAB triblock²⁸ copolymers can stabilize HCP over a wider region of phase space than monodisperse analogues. Although these levels of dispersity are

significantly higher than those found in FDF, F2DF, and F4DF (Table 1, Figure 1), we were inspired to investigate this effect in more detail. F4DF was selected as a representative example since it shows the largest region of HCP stability (Figure 2c). SCFT models were designed to include small amounts of molar mass dispersity in the F and 4D blocks that match the values measured experimentally (D = 1.04, see Table S6 and Figure S29). Free energies of the DIS, BCC, HCP, and FCC phases were computed at $\chi N = 40$ for these slightly disperse melts and compared to the monodisperse calculations described above (Figure S28). The stability windows of each phase are shown in Figure 6, which indicates small amounts of dispersity in all three blocks significantly widens the channel of HCP stability with a width ($\Delta f_F \sim 0.07$) comparable to that found in the experimental F4DF phase diagram ($\Delta f_{\rm F} \sim 0.05$, Figure 2c). Two mechanisms related to dispersity stabilize the HCP phase, which are revealed by examining the spatial distribution of different chains (Tables S7–S10). Density profile plots indicate short A blocks are relatively abundant at interstitial sites, meaning they pull out from spheres because of a low enthalpic penalty. However, a different mechanism for relaxing packing frustration is also present, whereby B blocks that are longer than average can extend to fill interstitial sites with a smaller entropic penalty than average-length B blocks. While these mechanisms have been known in the context of diblocks and triblocks with dispersity confined to one block, their effect is evidently amplified when operating in tandem as illustrated in Figure 7. Finally, we emphasize that the stabilization of HCP is seemingly related to molar mass (and accompanying composition) dispersity in the block copolymer chains; there is no evidence of homopolymer contamination in F4DF-27 as assessed using automated flash chromatography (Figures S30–S31).⁴³

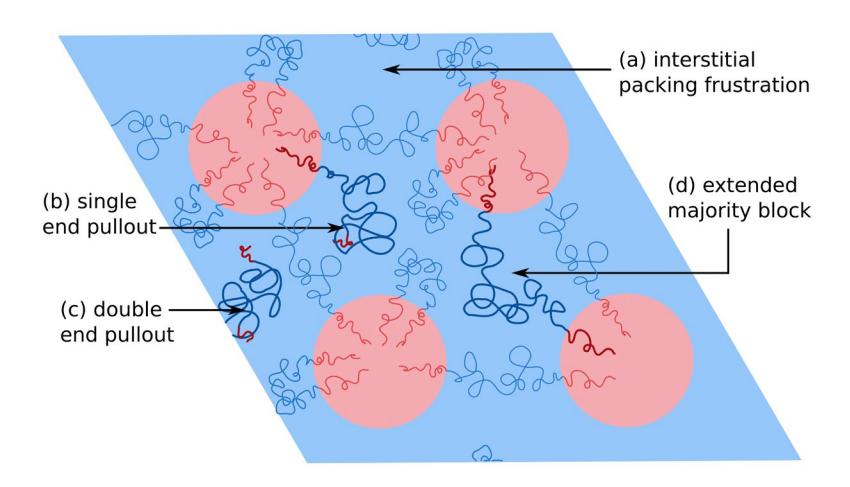


Figure 7. Proposed mechanisms that stabilize the HCP sphere phase in low-dispersity ABA triblock copolymer melts. Some (but not all) of these are also available in analogous AB diblock copolymers. (a) An interstitial site that average-length chains must stretch to fill, resulting in an entropic penalty. (b) A chain with one short end that has pulled out of a sphere, which can more easily reach interstitial sites. (c) A chain with two short ends that have pulled out of a sphere, allowing the entire molecule to migrate to an interstitial site. (d) A long B block, which can stretch to fill interstitial regions without experiencing a severe entropic penalty.

Our SCFT calculations capture the important role of block dispersity in stabilizing the HCP phase, but they do not explain the significant differences observed when comparing the experimental phase diagrams of FDF, F2DF, and F4DF. At present, we can only speculate as to the cause of this unexpected result. A potentially important consideration is the local packing behavior of B blocks near interstitial sites in the HCP unit cell. The branching present in the 2-dodecyl and 4-dodecyl repeat units could conceivably organize differently than straight alkyl chains in the linear dodecyl analog. This type of local liquid structure is not captured by SCFT, but it might be revealed in a fully fluctuating field-theoretic simulation. We emphasize that a wide, likely pure HCP window was also observed experimentally in 4DF diblock copolymer melts with $f_F = 0.23-0.29$ (Figure S11). SCFT calculations indicate analogous diblocks have a similar window

of predicted HCP stability ($f_F = 0.21$ –0.26, Figure S32), albeit slightly smaller than the triblock because there are fewer mechanisms available to relieve packing frustration (Figure 7). Together, these results suggest that architecture (AB vs. ABA) is not solely responsible for stabilizing HCP. Instead, the choice of monomer (4D or 2D) seems critical. A possible explanation lies in potential side reactions that occur during the synthesis of F2DF, F4DF, and 4DF. Tertiary carbons in the 2-dodecyl and 4-dodecyl repeat units may undergo hydrogen atom abstraction yielding side-chain radicals that can cause branching.⁴⁴ This behavior, which may not be obvious in size-exclusion chromatograms, could conceivably influence phase behavior, particularly given the sensitivity of self-assembly to small levels of dispersity as suggested by SCFT. Detailed nuclear magnetic resonance experiments might be sensitive enough to pick up such impurities.

CONCLUSIONS

In summary, pure hexagonally close-packed spheres are stable and accessible in linear ABA and AB block copolymer melts. Time- and temperature-dependent small angle X-ray scattering and dynamic mechanical thermal analysis experiments suggest HCP is an equilibrium phase since it forms reversibly under different processing conditions. The timescale associated with nucleating and growing the HCP phase from a supercooled liquid or soft solid is intermediate to σ and A15 with polymers of comparable molecular weights and volume fractions. However, unlike σ and A15, the HCP sphere phase forms without proceeding through an intermediate dodecagonal quasicrystal. Self-consistent field theory calculations indicate small amounts of molar mass dispersity ($D_{\text{total}} = 1.04$) help stabilize HCP when one block is composed of 2-dodecyl or 4-dodecyl acrylate. These results reveal design rules that can be used as the basis for the formation of unique morphologies in block copolymers, an important class of soft materials.

ASSOCIATED CONTENT

Supporting Information

Experimental procedures, representative molecular characterization data, selected SAXS patterns, representative time- and temperature-dependent SAXS and DMTA characterization, indexed SAXS patterns, and self-consistent field theory (SCFT) calculations.

AUTHOR INFORMATION

Corresponding Authors

Andrew K. Whittaker — Australian Institute for Bioengineering and Nanotechnology;

ARC Centre of Excellence in Convergent Bio-Nano Science and Technology, University of

Queensland, Brisbane, Queensland 4072, Australia; Email: *a.whittaker@uq.edu.au

Craig J. Hawker — Materials Research Laboratory, Materials Department, and Department of Chemistry & Biochemistry, University of California, Santa Barbara, California 93106, United States; Email: *hawker@mrl.ucsb.edu

Christopher M. Bates — Materials Department, Materials Research Laboratory,

Department of Chemical Engineering, and Department of Chemistry & Biochemistry,

University of California, Santa Barbara, California 93106, United States; Email:

*cbates@ucsb.edu

Authors

Cheng Zhang — Materials Research Laboratory, University of California, Santa Barbara,
California 93106, United State; Australian Institute for Bioengineering and

Nanotechnology, ARC Centre of Excellence in Convergent Bio-Nano Science and Technology, University of Queensland, Brisbane, Queensland 4072, Australia.

Daniel Vigil — Materials Research Laboratory, University of California, Santa Barbara, California 93106, United State.

Dan Sun — Materials Research Laboratory, University of California, Santa Barbara, California 93106, United State.

Morgan W. Bates — Materials Research Laboratory, University of California, Santa Barbara, California 93106, United State.

Tessa Loman — Materials Research Laboratory, University of California, Santa Barbara, California 93106, United State.

Elizabeth A. Murphy — Materials Research Laboratory, University of California, Santa Barbara, California 93106, United State.

Stephanie M. Barbon — Materials Research Laboratory, University of California, Santa Barbara, California 93106, United State.

Jung-Ah Song — Materials Research Laboratory, University of California, Santa Barbara, California 93106, United State.

Beihang Yu — Department of Chemical Engineering, University of California, Santa Barbara, California 93106, United State.

Glenn H. Fredrickson — Materials Research Laboratory, Materials Department, and Department of Chemical Engineering, University of California, Santa Barbara, California 93106, United States.

Notes

The authors declare no competing financial interest.

ACKNOWLEDGMENTS

The research reported here was supported by the National Science Foundation through the MRSEC Program under Award No. DMR-1720256 (IRG-3, G.H.F., C.J.H., C.M.B.) and under Award No. DMR-1844987 (C.M.B.). A.K.W. and C.Z. acknowledge support from the Australian Research Council (CE140100036) and National Health and Medical Research Council for an Early Career Fellowship (APP1157440 to C.Z.). The research reported here made use of shared facilities of the UC Santa Barbara Materials Research Science and Engineering Center (MRSEC, NSF DMR 1720256), a member of the Materials Research Facilities Network (www.mrfn.org). Use was made of computational facilities purchased with funds from the National Science Foundation (CNS-1725797) and administered by the Center for Scientific Computing (CSC). The CSC is supported by the California NanoSystems Institute and the Materials Research Science and Engineering Center (MRSEC; NSF DMR-1720256) at UC Santa Barbara. Use of the Stanford Synchrotron Radiation Lightsource is supported by the U.S. Department of Energy, Office of Science, Office of Basic Energy Sciences under Contract No. DE-AC02-76SF00515. The SSRL Structural Molecular Biology Program is supported by the DOE Office of Biological and Environmental Research, and by the National Institutes of Health, National Institute of General Medical Sciences (including P41GM103393). The authors acknowledge Pat Getty for assistance with preparing the table of contents figure.

REFERENCES

- 1. Young, D. A., *Phase diagrams of the elements*. University of California Press: Berkeley, Los Angeles, and Oxford: 1991.
- 2. De Graef, M.; McHenry, M. E., *Structure of Materials: An Introduction to Crystallography, Diffraction and Symmetry*. 2 ed.; Cambridge University Press: Cambridge, 2012.
- 3. Goodfellow, B. W.; Yu, Y.; Bosoy, C. A.; Smilgies, D.-M.; Korgel, B. A., The Role of Ligand Packing Frustration in Body-Centered Cubic (bcc) Superlattices of Colloidal Nanocrystals. *J. Phys. Chem. Lett.* **2015**, *6* (13), 2406-2412.
- 4. Kim, S. A.; Jeong, K.-J.; Yethiraj, A.; Mahanthappa, M. K., Low-symmetry sphere packings of simple surfactant micelles induced by ionic sphericity. *Proc. Natl. Acad. Sci. U. S. A.* **2017**, 201701608.
- 5. Bates, C. M.; Bates, F. S., 50th Anniversary Perspective: Block Polymers—Pure Potential. *Macromolecules* **2017**, *50* (1), 3-22.
- 6. Bates, F. S.; Hillmyer, M. A.; Lodge, T. P.; Bates, C. M.; Delaney, K. T.; Fredrickson, G. H., Multiblock Polymers: Panacea or Pandora's Box? *Science* **2012**, *336* (6080), 434-440.
- 7. Lee, S.; Bluemle, M. J.; Bates, F. S., Discovery of a Frank-Kasper σ Phase in Sphere-Forming Block Copolymer Melts. *Science* **2010**, *330* (6002), 349-353.
- 8. Bates, M. W.; Lequieu, J.; Barbon, S. M.; Lewis, R. M.; Delaney, K. T.; Anastasaki, A.; Hawker, C. J.; Fredrickson, G. H.; Bates, C. M., Stability of the A15 phase in diblock copolymer melts. *Proc. Natl. Acad. Sci. U. S. A.* **2019**, *116* (27), 13194-13199.
- 9. Chen, L.; Qiang, Y.; Li, W., Tuning Arm Architecture Leads to Unusual Phase Behaviors in a (BAB)5 Star Copolymer Melt. *Macromolecules* **2018**, *51* (23), 9890-9900.

- 10. Xie, N.; Li, W.; Qiu, F.; Shi, A.-C., σ Phase Formed in Conformationally Asymmetric AB-Type Block Copolymers. *ACS Macro Lett.* **2014**, *3* (9), 906-910.
- 11. Qiang, Y.; Li, W.; Shi, A.-C., Stabilizing Phases of Block Copolymers with Gigantic Spheres via Designed Chain Architectures. *ACS Macro Lett.* **2020**, 668-673.
- 12. Jiang, W.; Qiang, Y.; Li, W.; Qiu, F.; Shi, A.-C., Effects of Chain Topology on the Self-Assembly of AB-Type Block Copolymers. *Macromolecules* **2018**, *51* (4), 1529-1538.
- 13. Xie, Q.; Qiang, Y.; Chen, L.; Xia, Y.; Li, W., Synergistic Effect of Stretched Bridging Block and Released Packing Frustration Leads to Exotic Nanostructures. *ACS Macro Letters* **2020**, *9* (7), 980-984.
- 14. Matsen, M. W., Effect of Architecture on the Phase Behavior of AB-Type Block Copolymer Melts. *Macromolecules* **2012**, *45* (4), 2161-2165.
- 15. Matsen, M. W., Polydispersity-Induced Macrophase Separation in Diblock Copolymer Melts. *Phys. Rev. Lett.* **2007**, *99* (14), 148304.
- 16. Matsen, M. W.; Bates, F. S., Origins of Complex Self-Assembly in Block Copolymers. *Macromolecules* **1996**, *29* (23), 7641-7644.
- 17. Lee, S.; Leighton, C.; Bates, F. S., Sphericity and symmetry breaking in the formation of Frank–Kasper phases from one component materials. *Proc. Natl. Acad. Sci. U. S. A.* **2014,** *111* (50), 17723-17731.
- 18. Huang, Y.-Y.; Hsu, J.-Y.; Chen, H.-L.; Hashimoto, T., Existence of fcc-packed spherical micelles in diblock copolymer melt. *Macromolecules* **2007**, *40* (3), 406-409.
- 19. Matsen, M. W., Fast and accurate SCFT calculations for periodic block-copolymer morphologies using the spectral method with Anderson mixing. *Eur. Phys. J. E* **2009**, *30* (4), 361.

- 20. Hsu, N.-W.; Nouri, B.; Chen, L.-T.; Chen, H.-L., Hexagonal Close-Packed Sphere Phase of Conformationally Symmetric Block Copolymer. *Macromolecules* **2020**, *53* (21), 9665-9675.
- 21. Park, M. J.; Bang, J.; Harada, T.; Char, K.; Lodge, T. P., Epitaxial Transitions among FCC, HCP, BCC, and Cylinder Phases in a Block Copolymer Solution. *Macromolecules* **2004**, *37* (24), 9064-9075.
- 22. Jayaraman, A.; Zhang, D. Y.; Dewing, B. L.; Mahanthappa, M. K., Path-Dependent Preparation of Complex Micelle Packings of a Hydrated Diblock Oligomer. *ACS Cent. Sci.* **2019**, 5 (4), 619-628.
- 23. Hamley, I.; Pople, J.; Diat, O., A thermally induced transition from a body-centred to a face-centred cubic lattice in a diblock copolymer gel. *Colloid Polym. Sci.* **1998,** *276* (5), 446-450.
- 24. Bang, J.; Lodge, T. P.; Wang, X.; Brinker, K. L.; Burghardt, W. R., Thermoreversible, Epitaxial f c c↔ b c c Transitions in Block Copolymer Solutions. *Phys. Rev. Lett.* **2002**, *89* (21), 215505.
- 25. Chen, L.-T.; Chen, C.-Y.; Chen, H.-L., FCC or HCP: The stable close-packed lattice of crystallographically equivalent spherical micelles in block copolymer/homopolymer blend. *Polymer* **2019**, *169*, 131-137.
- 26. Huang, Y.-Y.; Chen, H.-L.; Hashimoto, T., Face-Centered Cubic Lattice of Spherical Micelles in Block Copolymer/Homopolymer Blends. *Macromolecules* **2003**, *36* (3), 764-770.
- 27. Matsen, M. W., Stabilizing New Morphologies by Blending Homopolymer with Block Copolymer. *Phys. Rev. Lett.* **1995,** *74* (21), 4225-4228.
- 28. Matsen, M. W., Comparison of A-block polydispersity effects on BAB triblock and AB diblock copolymer melts. *Eur. Phys. J. E* **2013**, *36* (4), 44.

- 29. Wang, S.; Xie, R.; Vajjala Kesava, S.; Gomez, E. D.; Cochran, E. W.; Robertson, M. L., Close-packed spherical morphology in an ABA triblock copolymer aligned with large-amplitude oscillatory shear. *Macromolecules* **2016**, *49* (13), 4875-4888.
- 30. Imaizumi, K.; Ono, T.; Kota, T.; Okamoto, S.; Sakurai, S., Transformation of cubic symmetry for spherical microdomains from face-centred to body-centred cubic upon uniaxial elongation in an elastomeric triblock copolymer. *J. Appl. Crystallogr.* **2003**, *36* (4), 976-981.
- 31. Moonshi, S. S.; Zhang, C.; Peng, H.; Puttick, S.; Rose, S.; Fisk, N. M.; Bhakoo, K.; Stringer, B. W.; Qiao, G. G.; Gurr, P. A.; Whittaker, A. K., A Unique (19)F MRI Agent for the Tracking of Non Phagocytic Cells In Vivo. *Nanoscale* **2018**, *10* (17), 8226-8239.
- 32. Zhang, C.; Kim, D. S.; Lawrence, J.; Hawker, C. J.; Whittaker, A. K., Elucidating the Impact of Molecular Structure on the 19F NMR Dynamics and MRI Performance of Fluorinated Oligomers. *ACS Macro Lett.* **2018**, *7* (8), 921-926.
- 33. Xu, H.; Greve, E. M.; Mahanthappa, M. K., Morphological Impact of Segment Dispersity in Lithium Salt-Doped Poly(styrene)/Poly(ethylene oxide) Triblock Polymers. *Macromolecules* **2019**, *52* (15), 5722-5734.
- 34. Matsen, M. W.; Thompson, R. B., Equilibrium behavior of symmetric ABA triblock copolymer melts. *J. Chem. Phys.* **1999**, *111* (15), 7139-7146.
- 35. Barbon, S. M.; Song, J.-A.; Chen, D.; Zhang, C.; Lequieu, J.; Delaney, K. T.; Anastasaki, A.; Rolland, M.; Fredrickson, G. H.; Bates, M. W.; Hawker, C. J.; Bates, C. M., Architecture Effects in Complex Spherical Assemblies of (AB)n-Type Block Copolymers. *ACS Macro Lett.* **2020**, 1745-1752.
- 36. Baez-Cotto, C. M.; Mahanthappa, M. K., Micellar Mimicry of Intermetallic C14 and C15 Laves Phases by Aqueous Lyotropic Self-Assembly. *ACS Nano* **2018**, *12* (4), 3226-3234.

- 37. Liu, M.; Qiang, Y.; Li, W.; Qiu, F.; Shi, A.-C., Stabilizing the Frank-Kasper Phases via Binary Blends of AB Diblock Copolymers. *ACS Macro Lett.* **2016**, *5* (10), 1167-1171.
- 38. Sun, Y.; Tan, R.; Ma, Z.; Gan, Z.; Li, G.; Zhou, D.; Shao, Y.; Zhang, W.-B.; Zhang, R.; Dong, X.-H., Discrete Block Copolymers with Diverse Architectures: Resolving Complex Spherical Phases with One Monomer Resolution. *ACS Cent. Sci.* **2020**, *6* (8), 1386-1393.
- 39. Bates, M. W.; Barbon, S. M.; Levi, A. E.; Lewis, R. M.; Beech, H. K.; Vonk, K. M.; Zhang, C.; Fredrickson, G. H.; Hawker, C. J.; Bates, C. M., Synthesis and Self-Assembly of ABn Miktoarm Star Polymers. *ACS Macro Lett.* **2020**, *9* (3), 396-403.
- 40. Gillard, T. M.; Lee, S.; Bates, F. S., Dodecagonal quasicrystalline order in a diblock copolymer melt. *Proc. Natl. Acad. Sci. U. S. A.* **2016**, *113* (19), 5167-5172.
- 41. Cavicchi, K. A.; Lodge, T. P., Self-Diffusion and Tracer Diffusion in Sphere-Forming Block Copolymers. *Macromolecules* **2003**, *36* (19), 7158-7164.
- 42. Kim, K.; Schulze, M. W.; Arora, A.; Lewis, R. M.; Hillmyer, M. A.; Dorfman, K. D.; Bates, F. S., Thermal processing of diblock copolymer melts mimics metallurgy. *Science* **2017**, *356* (6337), 520-523.
- 43. Zhang, C.; Bates, M. W.; Geng, Z.; Levi, A. E.; Vigil, D.; Barbon, S. M.; Loman, T.; Delaney, K. T.; Fredrickson, G. H.; Bates, C. M.; Whittaker, A. K.; Hawker, C. J., Rapid Generation of Block Copolymer Libraries Using Automated Chromatographic Separation. *J. Am. Chem. Soc.* **2020**, *142* (21), 9843-9849.
- 44. Heatley, F.; Lovell, P. A.; Yamashita, T., Chain Transfer to Polymer in Free-Radical Solution Polymerization of 2-Ethylhexyl Acrylate Studied by NMR Spectroscopy. *Macromolecules* **2001**, *34* (22), 7636-7641.